Lipidic Cubic Phases as a Versatile Platform for the Rapid Detection of Biomarkers, Viruses, Bacteria, and Parasites

*Jijo J. Vallooran, Stephan Handschin, Samyuktha M. Pillai, Beatrice N. Vetter, Sebastian Rusch, Hans-Peter Beck, and Raffaele Mezzenga**

Rapid and affordable detection of analytes is critical in diagnostic technologies, but current methods are typically expensive and unsuitable for field detection. Lipidic cubic phases are optically isotropic, transparent lyotropic liquid crystals (LC), containing highly confined water nanochannels in-between percolating lipid bilayers following defined space groups. Due to this nanoconfinement, the water in these systems provides a unique environment for chemical and enzymatic reactions. Here, it is shown that during the in meso peroxidase enzymatic reaction, the converted product crystallizes within the mesophase domains, generating a detectable birefringence signal and a new general assay principle is presented for the detection of an unprecedented vast class of analytes using such birefringence as sole optical output signal. By exploiting bienzymatic cascade reactions or introducing an enzyme-linked immunosorbent assay based on birefringence (Birefringent-ELISA), this approach is used for real-time detection of exemplary analytes, such as glucose and cholesterol, model pathogenic microorganisms, *Escherichia coli*, and viruses such as Ebola and HIV. It is also shown how the same technology enables the rapid, naked-eye screening of malaria infection via in meso detection of hemozoin crystallites. This new technology is general and readily adaptable to the rapid detection of virtually any type of analyte, such as disease biomarkers, viruses, bacteria, and parasites.

1. Introduction

Although a simple and inexpensive detection of analytes is seen as the major focus of most of the current diagnostic technologies,[1] conventional detection methods remain time consuming, mostly require sophisticated instruments and trained personnel.[2–4] Due to these constraints, rapid detection of target analytes using simple, affordable devices is the main focus of numerous studies.[5–7] Despite several advances in detection and identification of analytes,[7,8] there is still an urgent need for new techniques tackling detection issues, especially for applications outside the laboratory.[2,9,10]

In the present work, we offer a new concept to solve this issue by using lipidic cubic phases as a biosensing platform and by introducing a new convenient and general assay principle, based on the monitoring of birefringence within the ensued mesophases as the only output signal. We demonstrate that such birefringence generates during the enzymatic reaction from converted products within the lipid cubic phases, and it is a result of the unique water environment provided by the cubic mesophases to the enzymatic reaction. Indeed, when mixed with water, lipid-based surfactants self-assemble into different liquid crystalline symmetries such as lamellar, inverted hexagonal and bicontinuous cubic phases.[11] These mesophases have been used in controlled release[12] and delivery systems[13] and find diverse applications in food, cosmetics and pharmaceuticals.[11,13,14] They also provide an excellent matrix for the entrapment of proteins[15] and enzymes[16] due to their biocompatibility, the presence of both hydrophilic and hydrophobic environments and their thermodynamic stability in excess water.[17] Finally, due to their isotropic nature, they do not exhibit birefringence (i.e., a luminous bright signal) when observed in between cross-polarizers, making them optically transparent. In the following, we demonstrate the possibility of encapsulating the enzyme horseradish peroxidase (HRP) within the bicontinuous cubic phase, making use of the typical conversion of substrates for analytes detection.

Dr. J. J. Vallooran, S. Handschin, Prof. R. Mezzenga
Department of Health Science and Technology
ETH Zurich
Schmelzbergstrasse 9, CH-8092 Zurich, Switzerland
E-mail: raffaele.mezzenga@hest.ethz.ch
Dr. S. M. Pillai
Institute of Physiology
University of Zurich
CH-8057 Zurich, Switzerland
Dr. B. N. Vetter
Swiss National Center for Retroviruses
Institute of Medical Virology
University of Zurich
CH-8057 Zurich, Switzerland
Dr. S. Rusch, Prof. H.-P. Beck
Swiss Tropical and Public Health Institute
University of Basel
CH-4051 Basel, Switzerland

DOI: 10.1002/adfm.201503428

2. Results

2.1. Development of In Meso Birefringence during the Enzymatic Reaction in Nanoconfined Mesophase Domains

The inset of **Figure 1**a shows a picture of a transparent bicontinuous cubic phase sample just at the beginning of the enzymatic reaction. Over time, the peroxidase enzymatic reaction in the presence of H_2O_2 produced typical green (inset of Figure 1b), blue (inset of Figure 1c), and orange (inset of Figure 1d) colored products within the cubic phase, when runs separately with three different organic substrates: 2,2′-azino-bis(3-ethylbenzthiazoline-6-sulfonic acid) (ABTS), 3,3′,5,5′-tetramethylbenzidine (TMB), and *o*-phenylenediamine dihydrochloride (OPD), respectively. This confirms that immobilized HRP inside lipid cubic phases retains its activity and can catalyze specific color changes, depending on the appropriate substrate. Bright-field microscopy images before (Figure 1a) and after (Figure 1b–d) the enzymatic reaction appear similar. Interestingly, when analyzed between cross-polarized optical microscopy (POM), no birefringence was observed at the beginning of the enzymatic reaction (Figure 1e) as expected from the isotropic nature of the cubic phase, whereas a significant amount of birefringence was detectable after 3 h of enzymatic reaction (Figure 1f–h). The unique structure of the cubic phase with its two continuous water nanochannels separated by a lipid bilayer provides a unique platform for the immobilization of the enzyme in its active form, while allowing a fast diffusion of the substrate within the matrix.

A series of experiments lead us to the confirmation that this birefringence stems from the crystallization of the converted, oxidized product during the enzymatic reaction in the cubic phase. Small-angle X-ray scattering (SAXS) spectra of the cubic phase before and after the enzymatic reaction (Figure S1a, Supporting Information) show that the cubic phase remains essentially unchanged throughout the enzymatic reaction and confirms that the evolving birefringence does not arise from changes in the mesophase. After the enzymatic reaction, the sharp peak in the wide-angle X-ray scattering (WAXS) spectra at 1.42 $Å^{-1}$ (Figure S1b, Supporting Information) confirms the crystalline nature of the converted ABTS substrate. A control enzymatic reaction run on a cubic phase made of an alternative lipid (phytantriol), resistant to hydrolysis due to the lack of ester bonds,[17] shows the same evolution of birefringence (Figure S1c, Supporting Information), whereas enzymatic reactions run on a hydrogel made of gelatin shows no presence of evolution of birefringence (Figure S1d, Supporting Information), conclusively confirming that the birefringence only arises from the in meso crystallization of ABTS-converted substrate. Similarly, several alternative control experiments in which either HRP, H_2O_2 or the substrate was missing in the cubic phase to prevent enzymatic reactions produced no birefringence.

A typical UV–vis spectrum, taken during the peroxidase enzymatic reaction using ABTS as substrate (**Figure 2**a), identifies the initial steady-state region of the reaction, which further confirms the enzymatic reaction within the lipid cubic phase.[16,18] Then under the POM, we found that over the sequence of the reaction, birefringence started to develop,

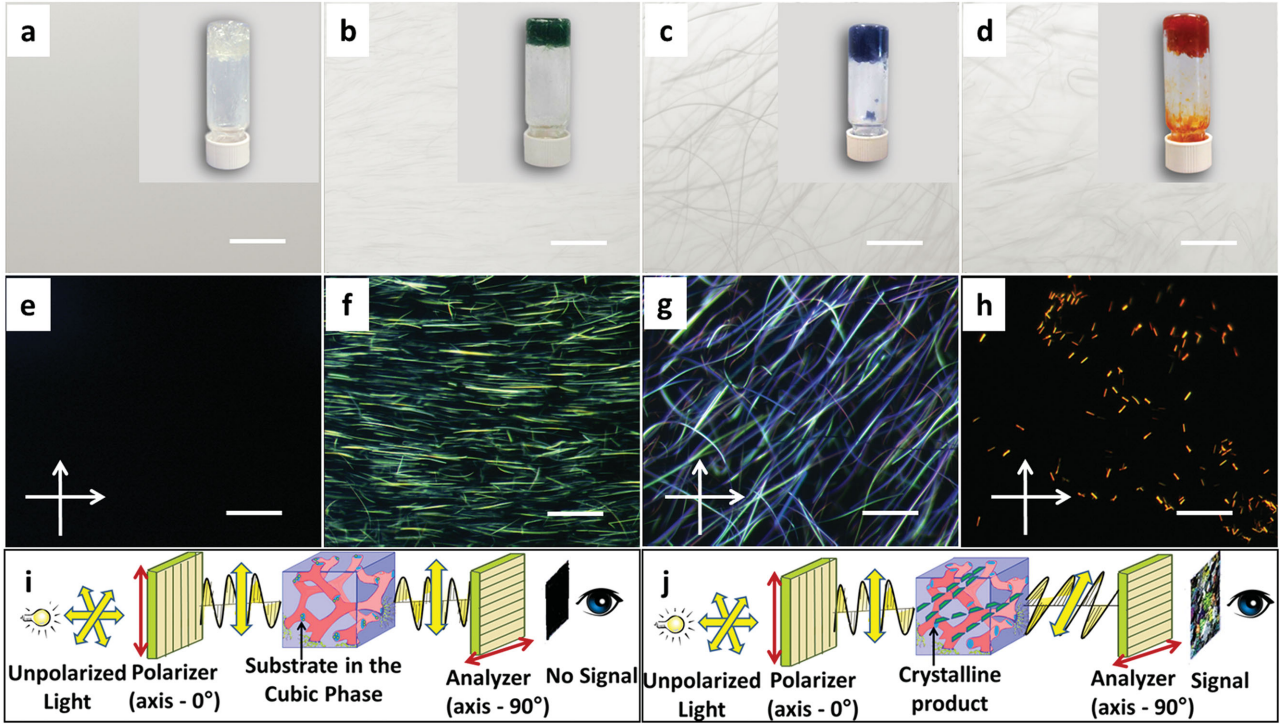

Figure 1. Light microscopy images a) before and b–d) after 3 h of enzymatic reaction using the substrate b) ABTS, c) TMB, and d) OPD. Insets show the visual appearance of each sample. The corresponding images in cross-polarized optical microscopy, e) before and f–h) after enzymatic reaction. Scale bar corresponds to 50 µm. Schematic of birefringence generation in isotropic cubic phases i) before and j) after the HRP enzymatic reaction. Crystallization of the converted product is responsible for the birefringence.

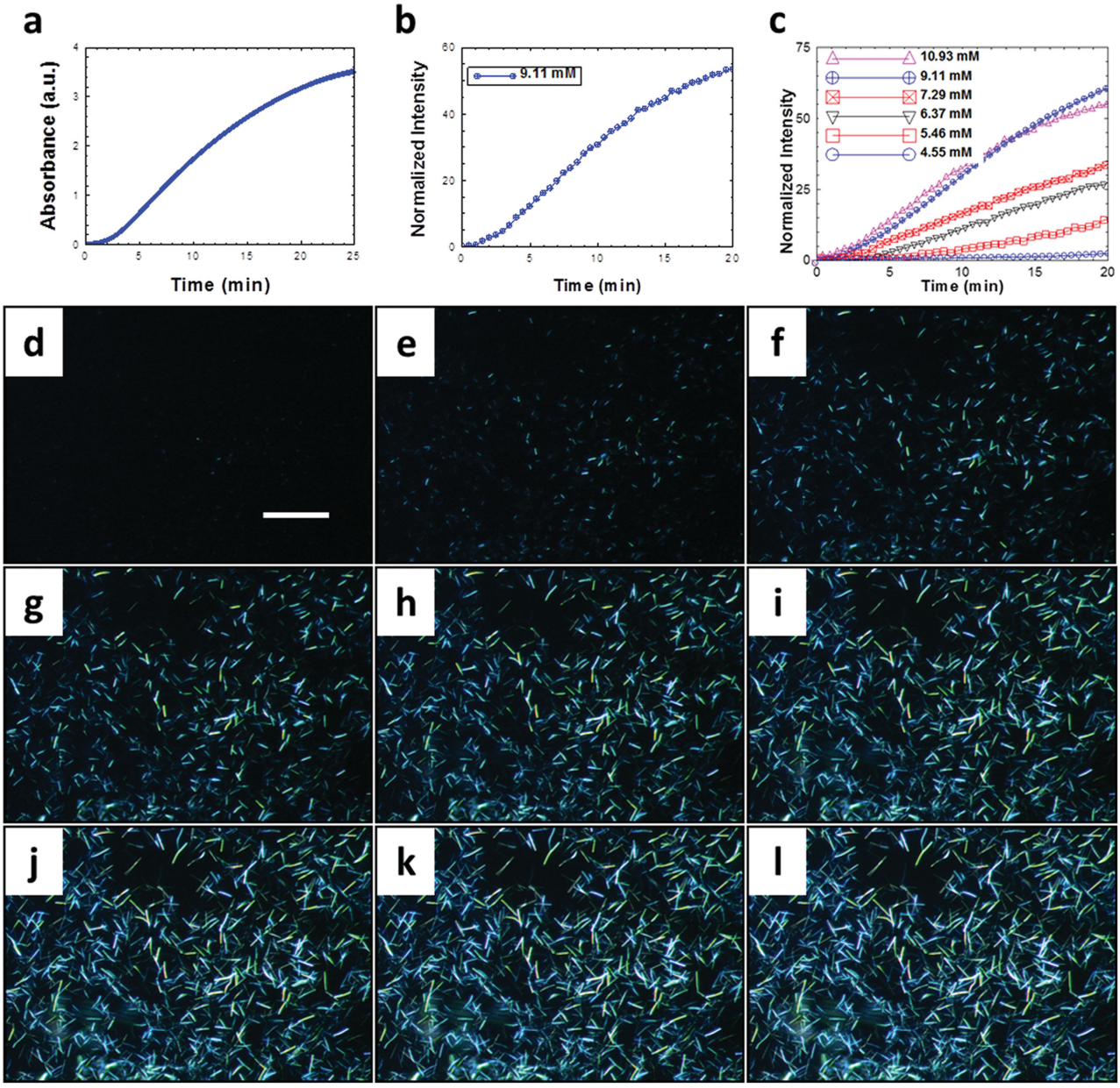

Figure 2. Illustration of real-time monitoring of an enzymatic reaction using birefringence. a) UV–vis spectra of the HRP enzymatic reaction with 9.118×10^{-3} M ABTS as substrate. b) Plot of the normalized birefringence intensity versus time arising from the conversion of 9.118×10^{-3} M ABTS. c) Plot of the normalized birefringence intensity versus time at different ABTS substrate concentrations. d–l) POM images of the cubic phase taken every 2 min during the enzymatic reaction with 9.118×10^{-3} M ABTS as substrate. Scale bar corresponds to 50 μm.

increased with time, and then slowly reached saturation. The normalized birefringence intensity with time follows the typical enzyme progression curve (Figure 2b), in direct analogy with the evolution of UV–vis spectra. The evolution of birefringence grows with increasing substrate concentration (Figure 2c), which is also consistent with the UV–vis spectra (Figure S2, Supporting Information). The observed lag time during the early stage of the enzymatic reaction, especially at the lowest concentrations of the substrate, is the result of the reduced relative diffusion rate of the substrate to the enzymatic reaction center in the highly viscous cubic phases, where diffusion is highly hindered and slowed down compared to bulk solutions.[16,18] The evolution of birefringence arising from the oxidized ABTS product allows the monitoring of the enzymatic reaction in real time by simple observation of the cubic phase under POM (Figure 2d–l). To the best of our knowledge, this is the first report showing that real-time monitoring of enzymatic reaction can be followed via the birefringence developed by an oxidized substrate. This phenomenon bears similarities with the fluorescence development during enzymatic reactions using

appropriate substrates[19–21] although the latter process requires specific fluorescent probes and given excitation wavelengths to be followed,[19] whereas birefringence development within cubic phases can be easily followed using cross-polarizers and shows a high degree of generality, being common to substrates such as ABTS and TMB. We did the same enzymatic reaction with identical concentrations of HRP, H_2O_2 and ABTS in free bulk water where no development of birefringence is detected. This clearly confirms the unique nature of the bicontinuous cubic phase in which the confined nanoenvironment of the hydrophilic/hydrophobic domains triggers the crystallization of the converted product responsible for the birefringence.

2.2. Bienzymatic Cascade Reaction for Real-Time Detection of Biomarkers

By following the same strategy discussed above, but using a bienzymatic cascade reaction, the development of birefringence can be followed to detect and quantify glucose concentration. There is a considerable interest in the medical industry[22] to efficiently measure glucose concentrations and there are significant worldwide efforts aiming at the development of new glucose monitoring methods.[22,23] To this end, we immobilized the two enzymes glucose oxidase (GOD) and HRP in the cubic phase (Figure S3a, Supporting Information). The GOD catalyses the conversion of β-D-glucose and oxygen to D-glucono-1,5-lactone and H_2O_2[24] (**Figure 3**a). The H_2O_2 arising from the first reaction then oxidizes ABTS in the presence of HRP, which in turn results in the formation of birefringence (Figure 3b–g). As shown in Figure 3h, the overall birefringence intensity generated by the oxidized product after 12 min reaction at 37 °C showed a linear increase with glucose concentration in the range of 3–8 × 10^{-3} M.

The detection of birefringence from an enzymatic cascade reaction is general enough to be scalable and adaptable to the detection of other molecules: we next showed its generality by applying the same concept on another model analyte, this time purely hydrophobic in nature: cholesterol. The measurement of cholesterol is also of key interest in clinical applications[25] because abnormal levels of cholesterol in blood can cause clinical disorders such as heart disease, hypertension, arteriosclerosis, and coronary artery disease.[26] Here, we used cholesterol oxidase (ChOD) and HRP to perform the bienzymatic cascade reaction[27] and the birefringence developed at 37 °C (Figure S3b–f, Supporting Information) showed again a perfectly linear correlation with the cholesterol concentration in the range of 10–30 × 10^{-3} M, as shown in Figure 3i. In contrast to the previous case, where glucose was solubilized in the water channels of the cubic phase, in the present case we solubilized cholesterol in the hydrophobic part of the cubic phase. This illustrates well how robust and general the present approach is, in which use of lipid-based lyotropic mesophases conveniently provides dual advantage of hydrophilic and hydrophobic domains within the same matrix.

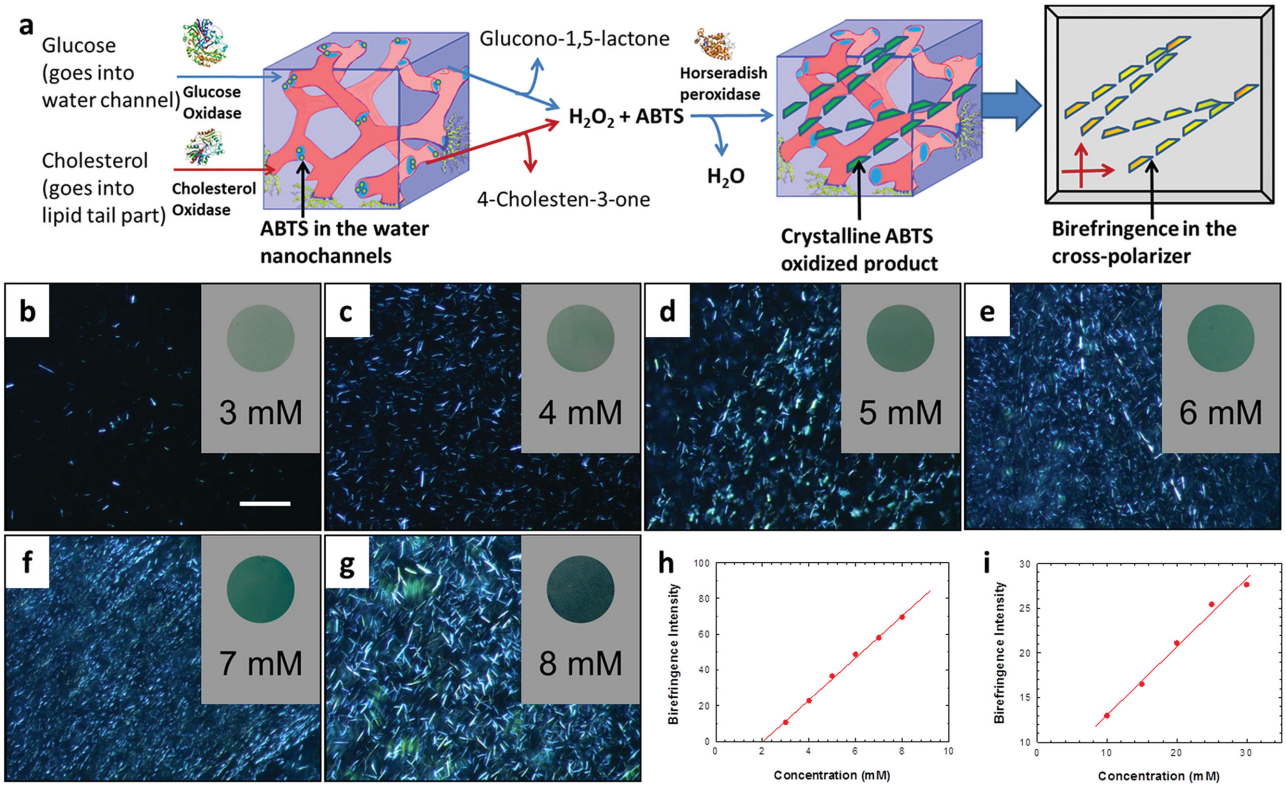

Figure 3. Illustration of the detection of glucose and cholesterol biomarkers by in meso birefringence development. a) Schematic representation of birefringence development after the enzymatic cascade reaction within the cubic phase. POM images of the cubic phase after 12 min of enzymatic reaction at 37 °C with b) 3, c) 4, d) 5, e) 6, f) 7, and g) 8 × 10^{-3} M glucose. Scale bar corresponds to 50 µm and applies to all images. Insets show the visual appearance of each sample. Linear dependence of the birefringence intensity versus h) glucose and i) cholesterol concentration.

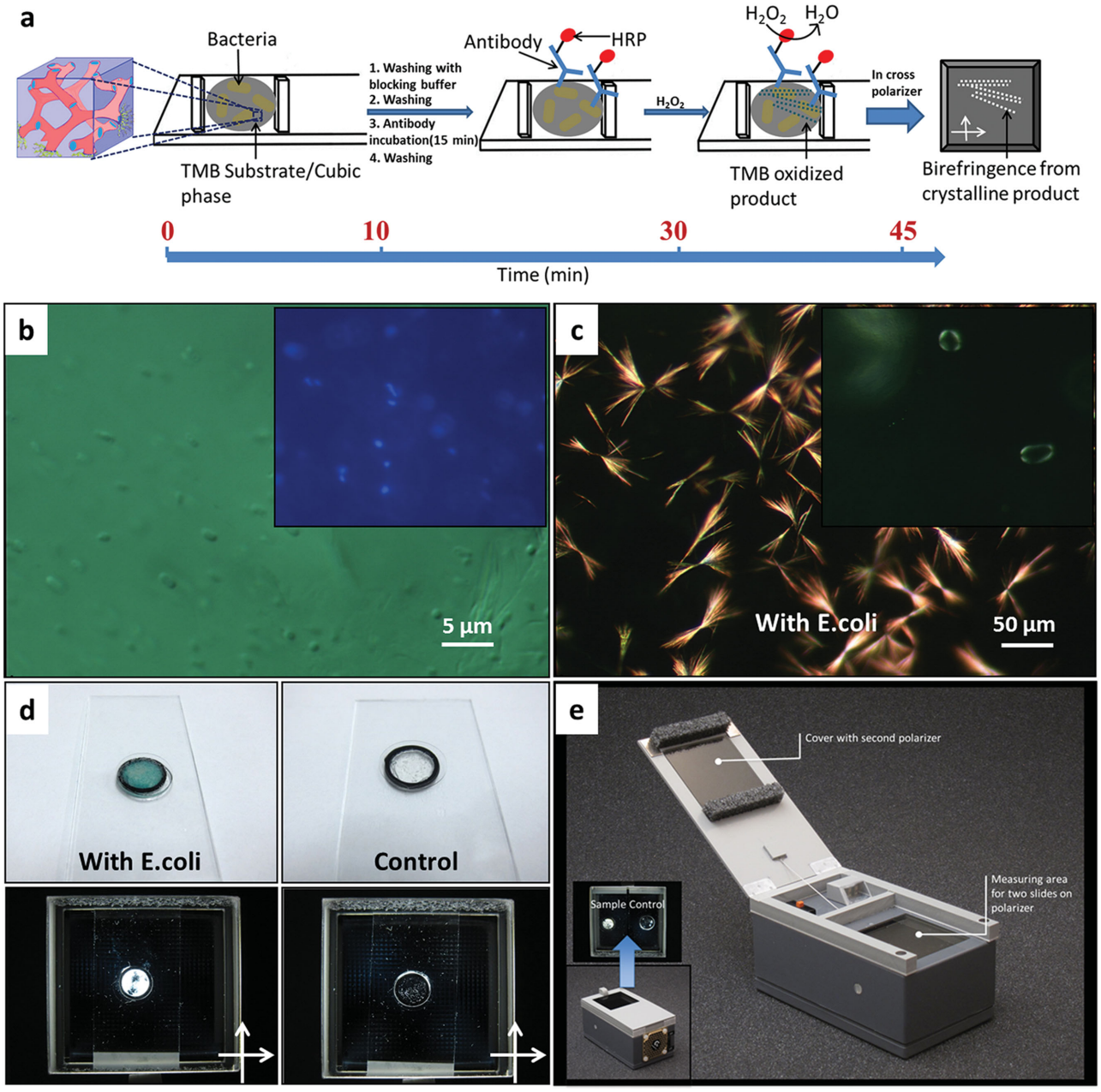

Figure 4. Illustration of bacteria detection. a) Schematic representation of birefringent ELISA. b) Light microscopy image of immobilized *E. coli* in the cubic phase. Inset shows a fluorescence microscopy image with DAPI. c) POM image after the birefringent ELISA at 37 °C. Inset shows a POM image of the control sample (no *E. coli*). d) Photographs of the samples on slides (top two images) and their visualization by the birefringent ELISA in the cross-polarized filter device (bottom two images) at 37 °C. e) Photograph of the portable birefringent ELISA device.

2.3. Birefringent ELISA for Detection of Bacteria and Viruses

In analogy with the use of HRP in immunoassay applications,[28] we next introduced the new birefringent enzyme-linked immunosorbent assay (ELISA) for the rapid detection of model food pathogens, exemplified here in the detection of *Escherichia coli*. ELISAs are possibly the most widely used tests due to their relative simplicity of diagnostic although they typically require hours for the detection process.[2,29] This type of assay based on the conversion of a substrate to a product is of vital importance in the detection of pathological microorganisms,[10] catalytic antibodies, and screening libraries of potential drugs and inhibitors.[30] A schematic representation of the birefringent ELISA method for pathogens detection is shown in **Figure 4**a. For this task, we used the hydrophobic substrate TMB, instead of the hydrophilic substrate ABTS, to avoid release of substrate from the cubic phase during the necessary washing procedure with buffer.

The rapid formation of the cubic phase (Figure S4a, Supporting Information) at room temperature by mixing *E. coli*

as suspension in water and the TMB-contained lipid ensures immobilization of *E. coli* and the solubilization of the substrate TMB in the mesophase. Light and fluorescence microscopy (Figure 4b) images confirm that *E. coli* is homogenously distributed in the mesophase. The mesophase-containing bacteria and TMB were incubated with HRP-conjugated antibody solution, followed by rinsing with buffer to leave only the antibodies bound to *E. coli* in the system. In the presence of H_2O_2, the antibody-bound HRP starts the enzymatic reaction, giving rise to color changes and the converted TMB product in the mesophase starts to crystallize, inducing birefringence in the mesophase (Figure 4c). Since the cubic phase is stable in excess of buffer, the analyte-bound HRP (conjugated to the antibody) will be in close contact with the cubic phase and the hydrophobic substrate TMB. This will ensure the crystallization of converted substrate within the cubic phase without its loss to the flushing buffer containing the HRP. No color or birefringence changes were observed in the control experiments lacking bacteria (inset of Figure 4c). Macroscopic birefringence (Figure 4d) can be visible to the naked eye using a simple, portable cross-polarized device (Figure 4e) with a cost of less than 20 Euros. One of the main disadvantages of the conventional ELISA is that the visual distinction between the noncolored and colored solution can only be achieved with confidence at high concentrations of the target analytes, whereas the naked eye detection using birefringence is independent of color, making it particularly appealing for initial qualitative screening for deadly pathogens[7,10] and also in resource-limited environments.[6,9]

The current method can also be utilized for the detection of viruses and here we illustrate the detection of HIV-1 virus-like particle (VLP) p24 antigen as a representative case of immediate relevance. Rapid detection of p24 antigen can be exploited for the early diagnosis of HIV infection in a cost-effective way, which is of prime importance in resource-limited regions where expensive nucleic acid-based tests might not be affordable. We designed an indirect ELISA assay for the detection and quantification of the model analyte HIV-1 capsid antigen p24 in human plasma in ≈1 h. Similarly to the above cases, we have used the birefringent ELISA to produce a simultaneous color change and birefringence (**Figure 5**a, 5b) within the cubic phase (Figure S4b, Supporting Information). Absence of birefringence in the POM (inset of Figure 5a) in five different control experiments (Figure S4c, Supporting Information) confirms the specificity of the detection.

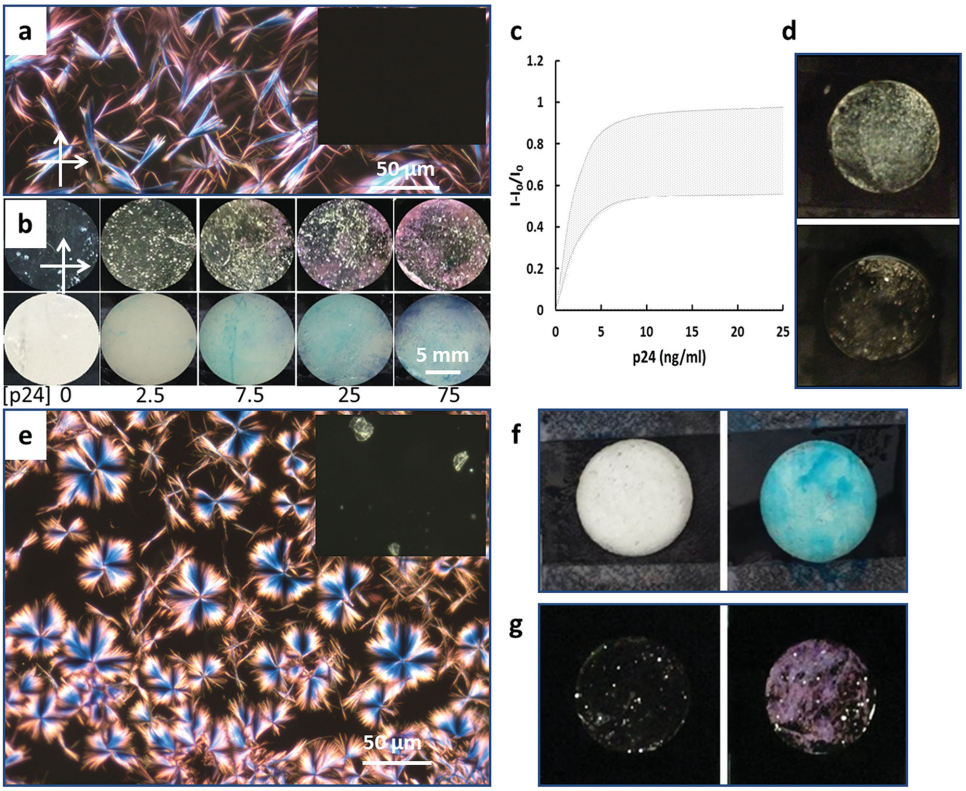

Figure 5. Illustration of virus detection. a) POM image of HIV p24 antigen containing VLP-spiked human plasma within the cubic phase after birefringent ELISA, at 37 °C. Inset shows the POM image of a control sample (the cubic phase made of only human plasma). b) Photographs of samples (bottom images) with different p24 concentrations in ng mL^{-1} and their visualization in the cross-polarized device after birefringent ELISA (top images) within the cubic phase at 37 °C. c) Experimental normalized birefringent intensity values associated with measured uncertainty range arising in the cubic phase at increasing p24 antigen concentration. d) Photographs of sample with 250 pg mL^{-1} HIV-1 p24 antigen after performing sandwich ELISA (top image) and the control sample (bottom image). e) POM image of a cubic phase containing Zaire Ebola virus glycoprotein after birefringent ELISA at 37 °C. Inset shows the POM image of a control sample. f) Photographs of cubic phase either containing (positive sample, left) or not (control, right), the Ebola virus glycoprotein after birefringent ELISA at 37 °C. g) As in (f), but visualized in between cross-polarizers in the portable birefringent device.

In the case of detection of HIV p24 antigen during chronic infections, heat treatment of plasma can increase the concentration of free p24 as the majority of antigen is bound in immune complexes.[31] The concentration of unbound antigen can be drastically increased by heating HIV-infected plasma to 100 °C for a short duration. Even though the heat-treated plasma in the bicontinuous cubic phase shows slight background birefringence signal in the POM (Figure S4d, Supporting Information), the birefringence developed after the ELISA method is significantly higher (Figure S4d (inset), Supporting Information), which further illustrates the potential of this method in a practical application of HIV detection.

This birefringence is dependent on the concentration of HIV p24 antigen (Figure 5b) and therefore can be used for the quantification of the analyte using the cross-polarized filter device. The measured birefringent intensities from each concentration (I) of p24 antigen and control sample (I_0) were calculated and the normalized intensity was used for quantification (Figure 5c). Differences in surface roughness of the gel may cause slight variations in the integrated birefringence intensity causing a relatively large standard deviation in the various assays. Although the limit of detection in the present birefringent ELISA method was 2.5 ng mL^{-1}, i.e., above the detection threshold of other more sophisticated methods, the simplicity of the proposed approach is anticipated to be of an unprecedented value for the rapid and inexpensive detection of HIV infections in resource-poor regions. Furthermore, the detection threshold can be improved by performing a slightly modified ELISA on the same device: as an example, we have increased the sensitivity by one order of magnitude (250 pg mL^{-1}) by simply performing a Sandwich ELISA, as shown in Figure 5d (see the Experimental Section). Though the current birefringent method is less sensitive than the colorimetric ELISA assays, it does provide a rapid, cost-effective, reliable POSITIVE/NEGATIVE detection, which is a primary need in the case of initial screens for infectious agents or deadly pathogens. This technology can be directly applied by incubation of blood or plasma on the top of capture antibody-immobilized mesophase-filled 96-well plates. Eventually, the readout of the device can also be carried out by connecting the device on a mobile phone for automated output (Figure S5, Supporting Information).

Similarly, in Figure 5e–g, we show how the same technology can be used for the detection of another devastating virus: the Ebola. Figure 5e shows the POM image of a mesophase containing the Ebola virus after a birefringent ELISA enzymatic reaction run at 37 °C for 1.5 h and the ensued birefringence. The absence of birefringence in the POM image of control experiments without the virus (inset of Figure 5e) again confirms the specificity of the detection. Figure 5f shows the visual appearance after the birefringent ELISA for both the positive (left) and the control (right) mesophases, whereas Figure 5g shows the same positive and control samples observed in the portable birefringent device.

3. Discussion

The water present within the nanochannels of the lipidic mesophases is highly confined with a majority of this water being bound to the polar heads of the lipids via hydrogen bonding,[32] as schematically sketched in **Figure 6**a. According to theoretical thermodynamic models, we may expect that less than 50% of water is free in the cubic phase nanochannels,[32] which is further supported by measurements based on broadband dielectric spectroscopy.[33] As a result, any chemical species dissolved within the water channels experiences a unique environment, which differs substantially from free bulk and unbound water. For example, Vauthey et al. have shown that the Maillard reaction run within the water nanochannels of lipid mesophases proceeds very differently for the homolog reaction in free bulk water.[34] Similarly, Sun et al. have recently demonstrated that the in meso peroxidase enzymatic kinetics follows different mechanisms compared to the same reaction run in bulk water.[18] Thus, it is the unique nanoconfined environment provided by the lipidic mesophases, which induces the crystallization of all the tested substrates after enzymatic conversion. This is unambiguously demonstrated by the fact that the same peroxidase enzymatic reaction, run in other types of gels where the greatest majority of water is free, does not produce any birefringence, i.e., the converted substrates remain water soluble (Figure S1d, Supporting Information).

Thus, the bicontinuous cubic phases serve as the ideal platform due to their isotropic and transparent nature combined to the high nanoconfinement of the lipid and water domains. Of course, if the analyte to be detected shows intrinsic birefringence, the method becomes highly suitable for immediate positive/negative screening because it is expected to increase birefringence by promoting aggregation. Here, we illustrate this by using this device for a label-free, naked-eye detection of *Plasmodium falciparum*, the devastating infectious pathogen causing malaria.[35] The protozoan *Plasmodium* parasite invades erythrocytes and digests hemoglobin. The heme

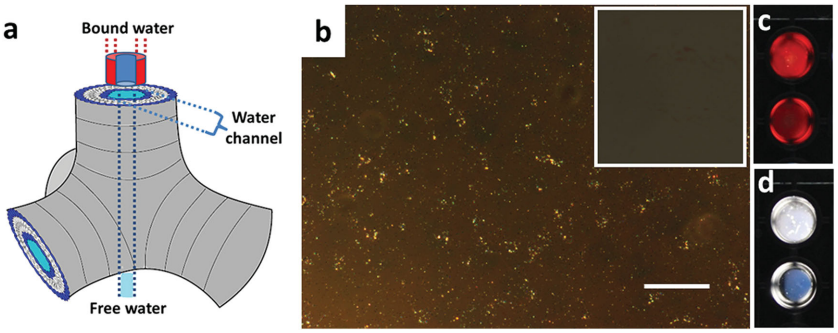

Figure 6. a) Schematic representation of free and bound water in a bicontinuous cubic phase. b) Cross-polarized optical microscopy image of a cubic mesophase produced using as hydrophilic component blood infected with *P. falciparum* parasites. The inset shows the negative control from a mesophase produced with uninfected blood. Scale bar corresponds to 50 µm. c) Photograph of two reservoirs in a 96-well plate, visually observed through the cross-polarized device, containing: (top image) a cubic mesophase produced using infected blood and (bottom image) the control negative sample. d) Photograph of two reservoirs in a 96-well plate, observed through the cross-polarized device, containing: (top image) a cubic mesophase produced using a buffer with extracted hemozoin and (bottom image) the control negative sample with uncontaminated buffer.

component, which is toxic to the parasites, is crystallized in the form of a brown birefringent crystal.[36] By detecting hemozoin directly, cross-polarized microscopy (Figure S7, Supporting Information) may be sufficient to diagnose malaria without any additional marker although this methodology remains difficult to be implemented in the field, especially in malaria-endemic areas, which often are resource limited.

In Figure 6b–6d, we show that in meso detection of hemozoin crystals is accessible to naked-eye screening. First, we checked that birefringence similar to that observed in infected blood (Figure S7, Supporting Information) under cross-polarized microscopy was also accessible in meso, when cubic phases were formed using blood infected with *P. falciparum* as a hydrophilic component (Figure 6b). After this had been successfully assessed, we moved forward to naked-eye detection of malaria infection by using the same portable device introduced in Figure 4. It has been reported that lipids and other hydrophobic constituents may enhance and stabilize hemozoin crystallization.[37] Enhancement of crystallization was in fact induced by the lipid mesophases, as shown by Figure 6c, where an intense birefringent signal was visually observed in few microliters of infected blood reconstituted in meso (Figure 6c, top image) as compared to a control sample of uninfected blood treated in the same way (Figure 6c, bottom image). The signal could be further enhanced by observing cubic mesophases produced directly with hemozoin suspensions extracted from *P. falciparum* cultures (Figure 6d, top image: positive; lower image: negative control). These results suggest that the observation of in meso birefringence in the portable device offers the potential for the rapid and inexpensive diagnosis of malaria using minimal blood volume and minimal sample preparation.

4. Conclusion

We have demonstrated that several substrates produce birefringence within lipid-based liquid crystal bicontinuous cubic phases, and that this birefringence development can be used to follow the enzymatic reaction in real-time. We engineered bienzymatic cascade reactions within the lipid mesophases and followed the birefringence development to detect glucose and cholesterol in a wide range of concentrations. Additionally, we combined peroxidase enzymatic reaction with antibody-mediated molecular recognition to detect pathogenic microorganisms and viruses, again, based on the sole detection of birefringence. We have finally shown how the intrinsic birefringence from hemozoin crystals produced by *P. falciparum* parasites can be enhanced in meso for the rapid diagnosis of malaria infection. The methodology proposed here exploiting both exogenously and endogenously generated in meso birefringence is general enough to be adapted to the detection of a vast class of analytes in a broad range of biotechnological fields and may pave the way to new detection strategies in the pharmaceutical, food, medical, and biothreat diagnostics.

5. Experimental Section

Enzymatic Reaction in Cubic Phase: The cubic phase system consists of an industrial grade of monolinolein (Dimodan U/J; Danisco, Denmark), blended with water.[38] HRP (Sigma-Aldrich) stock solution of 0.1 mg mL^{-1} was prepared in pH 7 phosphate buffer (Sigma-Aldrich), ABTS stock solution of 45.5×10^{-3} M was prepared in pH 4.65 (Sigma-Aldrich) acetate buffer, and 0.2 M H_2O_2 in pH 4.65 acetate buffer was prepared from 50% H_2O_2 solution in water (Sigma-Aldrich). A two-syringe (Hamilton)-coupled system was used for the preparation of the cubic phase at 37 °C.[39] In a typical preparation of the cubic phase, 375 mg of monolinolein was loaded together with 5 µL of enzyme stock solution in one syringe. In the other syringe, 100 µL of ABTS stock solution and 20 µL of H_2O_2 solution were loaded. The mixing of the solutions from the two syringes was carried out for 3 min through a narrow-connecting-coupled needle. This ensured the formation of a completely transparent cubic phase with homogenous distribution of the reactants. Final concentration of the enzyme was 5 µg mL^{-1}. Immediately after mixing, a green color and birefringence started to develop homogenously within the mesophase. The initial cubic phase was always prepared with a surfactant-to-water ratio of 75:25. For the assay with the substrate OPD (Sigma-Aldrich), the cubic phase was prepared in the same way using the OPD stock solution (55×10^{-3} M). Since the TMB (Sigma-Aldrich) substrate was not soluble in water, we solubilized TMB (20×10^{-3} M) in the lipid-loaded syringe. We also attempted at reproducing enzymatic reaction with other substrates such as pyrogallol (Sigma-Aldrich) and o-dianisidine (Sigma-Aldrich) but higher solubility of the converted product did not trigger any crystallization/birefringence.

Polarized Light Microscopy: A small amount of the cubic phase was analyzed under cross-polarized light using a Zeiss Axioskop 2 mot microscope at 37 °C.

UV–vis Measurement: Cubic phase samples from the syringe were directly transferred into a demountable UV cell (Starna, Type 20/C/Q/1) and measurements were carried out on a CARY-100 Bio UV–vis spectrophotometer at 37 °C.

SAXS and WAXS Measurements: SAXS and WAXS measurements were performed using a microfocused Rigaku X-ray source of wavelength $\lambda = 1.54$ Å, operating at 45 kV and 88 mA. The diffracted X-ray signal was collected either by a 2D argon-filled detector (for SAXS) or with the help of a Fuji Film BAS-MS 2025 imaging plate system: 15.2 × 15.2 cm, 50 µm resolution (for WAXS). For all measurements, the samples were placed inside a Linkam HFS91 hot stage and measured at 37 °C. Data were collected and averaged azimuthally to yield 1D intensity versus scattering vector q.

Enzymatic Cascade Reaction for Glucose Detection: The desired concentrations of β-D-glucose (Sigma-Aldrich) and ABTS (45.5×10^{-3} M) were prepared separately in pH 4.65 buffers. GOD (Sigma-Aldrich) stock solution of 0.1 mg mL^{-1} and HRP stock solution of 1 mg mL^{-1} were prepared in pH 7 phosphate buffer. 100 µL of β-D-glucose and 130 µL of ABTS were collected in one syringe, while 750 µL of monolinolein together with 10 µL of GOD and 10 µL of HRP was taken in another syringe and mixed through a needle connecting the two syringes as mentioned above. In the control sample, the β-D-glucose solution was replaced by 100 µL of buffer.

Enzymatic Cascade Reaction for Cholesterol Detection: The required concentration of cholesterol (Sigma-Aldrich) was directly solubilized in the monolinolein. ChOD (Sigma-Aldrich) stock solution of 0.2 mg mL^{-1} and HRP stock solution of 1 mg mL^{-1} were prepared in pH 7 phosphate buffer. 100 µL of buffer, 130 µL of ABTS, 10 µL of ChOD stock solution, and 10 µL of HRP stock solution were loaded in one syringe, while 750 mg of Dimodan together with the required concentration of cholesterol was loaded in the other syringe and mixed as described above. The control sample without cholesterol was prepared in the same way.

Bacteria: E. coli (K-12 MG 1655) was cultured overnight on nutrient agar at 37 °C. Then, single bacterial colonies were selected from LB agar and transferred into 5 mL LB media. After 5 h, 20 mL additional media were added and incubated overnight at 37 °C with shaking at 225 rpm. The following day, cells were pelleted (2500 g, 10 min) and washed with PBS and pelleted again. Bacteria were suspended as 107 mL^{-1} in pH 4.65 acetate buffer and used within 1 h after preparation.

Immobilization of Bacteria in the Cubic Phase: For the immobilization of *E. coli* in the cubic phase, one syringe was filled with 50 µL of *E. coli*

suspension in acetate buffer and the other syringe with 200 mg of monolinolein together with 2 mg of TMB. Mixing and preparation of the cubic phase was carried out via the double-connected syringes as mentioned before. The control samples were prepared without *E. coli*.

Observation of E. coli in Widefield Fluorescence Microscopy: E. coli in the cubic phase was stained with 1 μg mL^{-1} DAPI (4′, 6-diamidino-2-phenylindole) and imaging was carried out with a 100× oil immersion lens (NA 1.4) using the Zeiss filter set 02 for an excitation wavelength of 365–395 nm and a 420 nm long pass filter for the emission.

Birefringent ELISA for E. coli: An O-ring (1 mm thickness and 8 mm inner diameter) was filled with the mesophase mixed with bacteria (5×10^5/50 μL) and TMB and placed on a glass slide. The sample was washed with blocking buffer (5% BSA solution), followed by rinsing with the PBS buffer. HRP-conjugated primary antibody solution (Abcam ab68450, 1 mg mL^{-1}, dilution 1:100) was added on the mesophase and incubated for 15 min. After washing the mesophase three times with buffer, 0.05 M H_2O_2 was added to start the peroxidase reaction. A control sample was prepared in the same way without adding *E. coli*. The stability of the lipidic cubic phases in the presence of *E. coli*, H_2O_2, or other components needed to the birefringent ELISA detection was tested over 24 h prior to the onset of the enzymatic reaction (at time scales much longer than the detection kinetics) and the cubic phase remained the same, maintaining an identical lattice parameter as measured by X-ray scattering.

HIV-1 p24 Antigen Detection: Negative human plasma was spiked with various concentrations of noninfectious VLPs.[40] Efficient VLP lysis was achieved by mixing the VLP-spiked plasma with a previously described virus-disruption buffer[41] and incubating the sample for 10 min at room temperature. For heat-denatured samples, the VLP-spiked plasma was diluted 1:5 with PBS prior to incubation at 100 °C for 5 min. The aqueous part used to make bicontinuous cubic phase contains human plasma and VLPs, which contain the p24 antigen and lysis buffer. The hydrophobic substrate TMB is solubilized in the lipid surfactant, Dimodan, and then mixed with the aqueous part to form the cubic phase. This highly viscous cubic phase ensures the physical immobilization of the antigen p24 with in the mesophase and is then transferred into a glass slide with a neoprene spacer of 0.5 mm, which constitutes a microwell of 0.5 mm in height and 16 mm in diameter. It is then washed with PBS buffer and then incubated with blocking buffer (1% BSA solution) for 3 min. Mouse monoclonal anti-p24 (Aalto Bio Reagents, BC 1071, dilution 1:200, 5 μg mL^{-1}) is incubated for 25 min, followed by several washes with PBS buffer and then goat anti-mouse IgG conjugated to HRP (KPL, 474–1806, dilution 1:200, 5 μg mL^{-1}) is incubated for 25 min. Unbound antibody is then washed away and the introduction of 0.05 M H_2O_2 on the mesophase promoted the start of enzymatic reaction, yielding a simultaneous color change and birefringence with in the cubic phase. To minimize roughness effects, a second glass cover slip (ϕ = 18 mm) is always placed on the top of the incubated lipidic phase to smooth the signal prior data acquisition. Different control experiments were also performed (Figure S4c, Supporting Information). For sandwich ELISA, sheep anti-HIV-1 p24 is used as capture antibody (Aalto Bio Reagents, D 7320, dilution 1:100, 1 mg mL^{-1}) and mixed with TMB-solubilized Dimodan to yield the cubic phases. It is washed with the blocking buffer and then 250 pg mL^{-1} p-24 antigen is added on the top of the mesophases and incubated for 45 min. The mesophase is then washed with the PBS buffer. The incubation with the primary and secondary antibodies and birefringence generation occurs as described earlier for the standard birefringent ELISA.

Conversion of Birefringence Intensity into Analytical Signal: To start, we perform the birefringent ELISA on cubic phases containing the analyte, and thus generating a growing birefringence versus time, as well as on control inert samples. Both positive and control samples are placed in the cross-polarized filter device and digital images are taken over time at the same exposure and magnification in both sample series. The final intensity is calculated for the sample (I) and for the control (I_0) by calculating average pixel intensity of the digital image using image J software. The normalized intensity $I–I_0/I_0$ is plotted either versus time or versus different concentrations of the analytes.

Ebola Virus Glycoprotein Detection: The hydrophobic substrate TMB (2.1 mg) is solubilized in the 210 mg lipid surfactant, Dimodan, and then mixed with the 90 μL of buffer solution, which contains recombinant Zaire Ebola virus glycoprotein (Alpha Diagnostics, EVGP18-R-10) to form the cubic phase. Final concentration for Ebola virus glycoprotein was 30 ng mL^{-1}. This is then transferred into a glass slide with a neoprene spacer of 0.5 mm, which constitutes a microwell of 0.5 mm in height and 16 mm in diameter. It is then washed with PBS buffer and then incubated with blocking buffer (5% BSA solution) for 15 min. Rabbit anti-Zaire Ebola virus glycoprotein (Alpha Diagnostics, EVGP16-A, dilution 1:200) is incubated for 40 min, followed by several washes with PBS buffer and then Goat anti-rabbit poly-HRP (Life technologies, 32 260, dilution 1:200, 0.5 mg mL^{-1}) is incubated for 30 min. Unbound antibody is then washed away and the introduction of H_2O_2 on the mesophase promoted the enzymatic reaction to start, yielding a simultaneous color change and birefringence within the cubic phase. Different control experiments without Zaire Ebola virus glycoprotein, nonselective antibodies, etc. were performed in analogy to the detection of other analytes considered.

P. falciparum Culture: The *P. falciparum* 3D7 strain was cultured in vitro in human 0+ erythrocytes at 5% hematocrit as described,[42] using RPMI medium containing 0.5% Albumax.[43] Parasites were synchronized with 5% sorbitol as described.[44] Cultures were harvested by centrifugation and lysed in hypotonically in H_2O. 100 μL of this lysed culture is then added on top of 50 mg of phytantriol lipid, allowing 3 min to form the cubic mesophases in a 96-well plate.

Hemozoin Crystallites from P. falciparum Culture: 30 mL *P. falciparum* culture (7% late-stage parasitemia) was pelleted and lysed in 5 mL doubledistilled water (ddH_2O) at room temperature for 5 min. The lysate was centrifuged at 3500 g for 10 min. The pellet was dissolved in 2% SDS and vortexed vigorously. The lysate was centrifuged for 10 min at 21 000 g. The resulting hemozoin pellet was twice washed in ddH_2O and stored in 500 μL ddH_2O at room temperature. 100 μL of this ddH_2O suspension was then added on top of 50 mg of phytantriol lipid, allowing 3 min to form the cubic mesophases in a 96-well plate.

The control sample contained 500 μL uninfected human erythrocytes lysed in 1.5 mL ddH_2O.

Supporting Information

Supporting Information is available from the Wiley Online Library or from the author.

Acknowledgements

The authors would like to acknowledge ETH Zurich for the pioneer fellowship for financial support and Prof. Jörg Schüpbach, UZH, for valuable discussions on HIV experiments. J.J.V. and R.M. declare to be inventors of a patent filed by ETH Zurich related to the work presented here. This work is the recipient of the 2014 ETH Zurich Pioneer Fellowship.

Received: August 14, 2015
Revised: October 2, 2015
Published online: December 4, 2015

[1] E. C. Alocilja, S. M. Radke, *Biosens. Bioelectron.* **2003**, *18*, 841.
[2] A. S. Daar, H. Thorsteindottir, D. K. Martin, A. C. Smith, S. Nast, P. A. Singer, *Nat. Genet.* **2002**, *32*, 229.
[3] O. Lazcka, F. J. D. Campo, F. X. Muñoz, *Biosens. Bioelectron.* **2007**, *22*, 1205.
[4] P. Leonard, S. Hearty, J. Brennan, L. Dunne, J. Quinn, T. Chakraborty, R. Kennedy, *Enzyme Microb. Technol.* **2003**, *32*, 3.

[5] V. K. Gupta, J. J. Skaife, T. B. Dubrovsky, N. L. Abbott, *Science* **1998**, *279*, 2077.
[6] R. J. Carlton, J. T. Hunter, D. S. Miller, R. Abbasi, P. C. Mushenheim, L. N. Tan, N. L. Abbott, *Liq. Cryst. Rev.* **2013**, *1*, 29.
[7] S. K. Sia, V. Linder, B. A. Parviz, A. Siegel, G. M. Whitesides, *Angew. Chem.* **2004**, *43*, 498.
[8] C. J. Woolverton, G. D. Niehaus(Kent State University), *US Patent No. 7407815 B2*, **2008**.
[9] H. D. Sikes, R. R. Hansen, L. M. Johnson, R. Jenison, J. W. Birks, K. L. Rowlen, C. N. Bowman, *Nat. Mater.* **2008**, *7*, 52.
[10] R. De la Rica, M. M. Stevens, *Nat. Nanotechnol.* **2012**, *7*, 821.
[11] C. Fong, T. Le, C. J. Drummond, *Chem. Soc. Rev.* **2012**, *41*, 1297.
[12] J. J. Vallooran, R. Negrini, R. Mezzenga, *Langmuir* **2013**, *29*, 999.
[13] A. Angelova, B. Angelov, R. Mutafchieva, S. Lesieur, P. Couvreur, *Acc. Chem. Res.* **2011**, *44*, 147.
[14] S. B. Rizwan, B. J. Boyd, T. Rades, S. Hook, *Expert Opin. Drug Delivery* **2010**, *7*, 1133.
[15] A. Zabara, R. Mezzenga, *Soft Matter* **2012**, *8*, 6535.
[16] D. Li, M. Caffrey, *Proc. Natl. Acad. Sci. USA* **2011**, *108*, 8639.
[17] W.-K. Fong, T. Hanley, B. J. Boyd, *J. Controlled Release* **2009**, *135*, 218.
[18] W. Sun, J. J. Vallooran, A. Zabara, R. Mezzenga, *Nanoscale* **2014**, *6*, 6853.
[19] S. Kiyonaka, K. Sada, I. Yoshimura, S. Shinkai, N. Kato, I. Hamachi, *Nat. Mater.* **2004**, *3*, 58.
[20] A. Hennig, H. Bakirci, W. M. Nau, *Nat. Methods* **2007**, *4*, 629.
[21] S. D'Auria, J. R. Lakowicz, *Curr. Opin. Biotechnol.* **2001**, *12*, 99.
[22] C. E. Ferrante do Amaral, B. Wolf, *Med. Eng. Phys.* **2008**, *30*, 541.
[23] H. Shibata, Y. J. Hoe, T. Okitsu, Y. Matsunaga, T. Kawanishi, S. Takeuchi, *Proc. Natl. Acad. Sci. USA* **2010**, *42*, 17894.
[24] W.-J. Zhu, D. Q. Feng, M. Chen, Z. D. Chen, R. Zhu, H. L. Fang, W. Wang, *Sensor Actuat. B-Chem.* **2014**, *190*, 414.
[25] S. K. Arya, M. Datta, B. D. Malhotra, *Biosens. Bioelectron.* **2008**, *23*, 1083.
[26] F. R. Maxfield, I. Tabas, *Nature* **2005**, *438*, 612.
[27] R. Li, C. Xiong, Z. Xiao, L. Ling, *Anal. Chim. Acta* **2012**, *724*, 80.
[28] A. M. Azevedo, V. C. Martins, D. M. F. Prazeres, V. Vojinović, J. M. S. Cabral, L. P. Fonseca, *Biotechnol. Annu. Rev.* **2003**, *9*, 199.
[29] C.-M. Cheng, A. W. Martinez, J. Gong, C. R. Mace, S. T. Phillips, E. Carrilho, K. A. Mirica, G. M. Whitesides, *Angew. Chem.* **2010**, *49*, 4771.
[30] N. Sordé, G. Das, S. Matile, *Proc. Natl. Acad. Sci. USA* **2003**, *100*, 11964.
[31] J. Schüpbach, J. Böni, *J. Virol. Methods* **1993**, *43*, 247.
[32] W. B. Lee, R. Mezzenga, G. H. Fredrickson*Phys. Rev. Lett.* **2007**, *99*, 187801.
[33] S. Ezrahi, I. Nir, A. Aserin, N. Kozlovich, Y. D. Feldman, N. Garti, *J. Dispersion Sci. Technol.* **2002**, *23*, 351.
[34] S. Vauthey, C. Milo, P. Frossard, N. Garti, M. E. Leser, H. J. Watzke, *J. Agric. Food Chem.* **2000**, *48*, 4808.
[35] W. K. Peng, T. F. Kong, C. S. Ng, L. Chen, Y. Huang, A. A. S. Bhagat, N.-T. Nguyen, P. R. Preiser, J. Han, *Nat. Med.* **2014**, *20*, 1069.
[36] C. Wongsrichanalai, M. J. Barcus, S. Muth, A. Sutamihardja, W. H. A Wernsdorfer, *Am. J. Trop. Med. Hyg.* **2007**, *77*, 119.
[37] N. T. Huy, Y. Shima, A. Maeda, T. T. Men, K. Hirayama, A. Hirase, A. Miyazawa, K. Kamei, *PLoS ONE* **2013**, *8*, e70025.
[38] R. Mezzenga, C. Meyer, C. Servais, A. I. Romoscanu, L. Sagalowicz, R. C. Hayward, *Langmuir* **2005**, *21*, 3322.
[39] A. Cheng, B. Hummel, H. Qiu, M. Caffrey, *Chem. Phys. Lipids* **1998**, *95*, 11.
[40] R. Zufferey, D. Nagy, R. J. Mandel, L. Naldini, D. Trono, *Nat. Biotechnol.* **1997**, *15*, 871.
[41] J. Schüpbach, Z. Tomasik, M. Knuchel, M. Opravil, H. F. Günthard, D. Nadal, J. Böni, *J. Med. Virol.* **2006**, *78*, 1003.
[42] W. Trager, J. B. Jenson, *Nature* **1978**, *273*, 621.
[43] A. Dorn, R. Stoffel, H. Matile, A. Bubendorf, R. G. Ridley, *Nature* **1995**, *374*, 269.
[44] C. Lambros, J. P. Vanderberg, *J. Parasitol.* **1979**, *65*, 418.